Targeted delivery of liquid microvolumes into the lung

Jinho Kim[a], John D. O'Neill[a], N. Valerio Dorrello[b], Matthew Bacchetta[c], and Gordana Vunjak-Novakovic[a,d,1]

[a]Department of Biomedical Engineering, Columbia University, New York, NY 10027; [b]Department of Pediatrics, Columbia University, New York, NY 10029; [c]Department of Surgery, Columbia University, New York, NY 10032; and [d]Department of Medicine, Columbia University, New York, NY 10032

The ability to deliver drugs to specific sites in the lung could radically improve therapeutic outcomes of a variety of lung diseases, including cystic fibrosis, severe bronchopneumonia, chronic obstructive pulmonary disease, and lung cancer. Using conventional methods for pulmonary drug administration, precise, localized delivery of exact doses of drugs to target regions remains challenging. Here we describe a more controlled delivery of soluble reagents (e.g., drugs, enzymes, and radionuclides) in microvolume liquid plugs to targeted branches of the pulmonary airway tree: upper airways, small airways (bronchioles), or the most distal alveoli. In this approach, a soluble liquid plug of very small volume (<1 mL) is instilled into the upper airways, and with programmed air ventilation of the lungs, the plug is pushed into a specific desired (more distal) airway to achieve deposition of liquid film onto the lung epithelium. The plug volume and ventilation conditions were determined by mathematical modeling of plug transport in a tubular geometry, and targeted liquid film deposition was demonstrated in rat lungs by three different in vivo imaging modalities. The experimental and modeling data suggest that installation of microvolumes of liquid into a ventilated pulmonary airway could be an effective strategy to deliver exact doses of drugs to targeted pathologic regions of the lung, especially those inaccessible by bronchoscopy, to increase in situ efficacy of the drug and minimize systemic side effects.

pulmonary drug delivery | lung disease | liquid instillation | lung airway | alveoli

Effective treatment strategies for lung diseases such as cystic fibrosis, tuberculosis, bronchopneumonia, and lung cancer would involve a small, highly concentrated dose of drug delivered directly to the pathologic site (1, 2). Unfortunately, delivery of a precise drug dose to specific sites in the lung is challenging using conventional systemic drug administration methods, resulting in inefficient treatments for many lung diseases (3, 4). For example, orally administered drugs often require high doses to achieve therapeutic effects due to first-pass metabolism, which in turn leads to systemic side effects (5). Although drugs administered i.v. can avoid first-pass metabolism, they can still incur a range of side effects (6).

On the other hand, inhalation of aerosolized drugs has the advantage of noninvasively bringing a drug locally into the lung, and so it has been a first-line treatment option for many lung diseases in the outpatient setting (7, 8). In particular, dry powder inhalers can allow for local delivery of drugs in specific lung regions (9). Because properties of powders such as particle size, density, and cohesiveness strongly affect particle transport behavior, dry powders should be prepared with appropriate properties conducive to delivery into specific locations in the structurally complex pulmonary airway tree (10).

Alternatively, microvolumes of a liquid plug containing the drug could be instilled into the lung using an airway catheter or bronchoscope, distributed across the airway epithelium, and absorbed locally (11, 12). This liquid plug instillation approach has been an effective delivery method for surfactant replacement therapy, in which microliters of pharmaceutical pulmonary surfactant are instilled into the lungs to treat respiratory distress syndrome (13–16). Although the plug instillation approach is rather invasive and more suitable for treatment in the inpatient

setting, improved therapeutic effect could be achieved with minimal systemic absorption and more precise determination of the effective drug dose (12). Because a very small liquid volume is required in this process, potential flow-induced damage to delicate airway structures could be significantly reduced (17). Although liquid plug instillation may have great therapeutic potential, its applications have not been explored, largely because of limited understanding of the transport of liquid plugs in a ventilated lung.

We hypothesized that a simple modulation of the initial liquid plug volume and ventilation parameters would allow for the precise localized delivery of drugs to specific targeted regions of the lung, for optimal therapeutic effect. To this end, we conducted experimental and theoretical studies of plug transport and film deposition in a simple tubular geometry (e.g., glass capillary tube) to develop a theoretical foundation for liquid plug transport and to establish relationships between tube geometry, plug volume, and ventilation parameters. Based on these findings, we developed a mathematical framework for delivering therapeutic agents by film deposition onto targeted generations of the pulmonary airway tree. Because the ability to translate the findings for plug motion in capillary tubes to the behavior of instilled liquids in the actual lung airway is not obvious, we conducted extensive experimental studies in a rat model. By selecting the plug volumes and ventilation parameters according to our mathematical model, we demonstrated deposition of liquid film in targeted regions of the rat lung using three different imaging modalities. We report here the conditions and methods for delivering drug solutions into targeted regions of the lung.

Results

Liquid Plug Instillation and Delivery into Targeted Regions of the Pulmonary Airway. For liquid plug instillation and pressure-induced advancement, the initial plug volume and ventilation airflow rate

determine how deep into the lung a liquid plug will travel (Fig. 1A). Liquid film can be deposited on the specific airway surfaces according to the following series of steps: (i) A liquid plug introduced into an airway (rat trachea in this study; clinically, a bronchus of the human lung via catheter) is moved deeper into the lung by positive air pressure. As the plug travels through the airway, it deposits a thin film on the airway surface and splits into smaller plugs at bifurcations in downstream airways. (ii) During inspiration, the instilled plug progresses, splitting into increasingly smaller plugs at bifurcations while leaving a thin liquid layer along the airway surfaces. (iii) The plugs rupture before the end of the first inspiration, resulting in the generation of a liquid film in the target airway, which can be specified by selecting the plug volume and airflow rate. (iv) To deposit liquid into the deeper lung, liquid plugs are instilled such that they rupture in smaller airways, where airway diameters change significantly during ventilation, allowing plug reformation. With repeated plug transport, rupture, and reformation, film deposits all of the way into the alveoli (Fig. 1B).

Transport of liquid film on airway surfaces. Movement of liquid film deposited on airway surfaces can be induced by surface tension gradients and gravity (18). If the surface tension σ of the instilled liquid is lower than the endogenous fluid lining of the airway surfaces [e.g., pulmonary mucus, $\sigma < 30$ mN/m (19); surfactant, $\sigma < 10$ mN/m (20)], the surface tension gradient can further assist the film movement toward distal airways (i.e., by Marangoni flow) (21). However, if the instilled liquid has higher surface tension than the pulmonary lining [e.g., aqueous solution, $\sigma \sim 70$ mN/m (22)], the liquid film would not advance beyond the rupture site unless it

reforms into a plug, which can be pushed by pressure. When the film thickness is considerable, the film may flow in the direction of gravity (Fig. 1C).

Pulmonary airway model for liquid delivery. The pulmonary airways can be classified into the proximal ($G_0–G_{15}$) and the distal ($G_{16}–G_{23+}$), depending on their distance from the trachea, where G_N is the Nth airway generation (23–25). The proximal airways can be further divided into large ($G_0–G_5$) and small ($G_6–G_{15}$) airways, based on diameter. Notably, the diameter of the rat trachea $G_0 \sim 3.4$ mm is comparable to the diameter of human bronchioles G_5, whereas the small airways of the rat lung roughly correspond to the distal airways of the human lung (26). With modifications that account for human airway structures and airflow conditions, as well as airway surface properties, the mathematical model developed for liquid delivery in the rat lung could be adapted to the human lung (Fig. 1D).
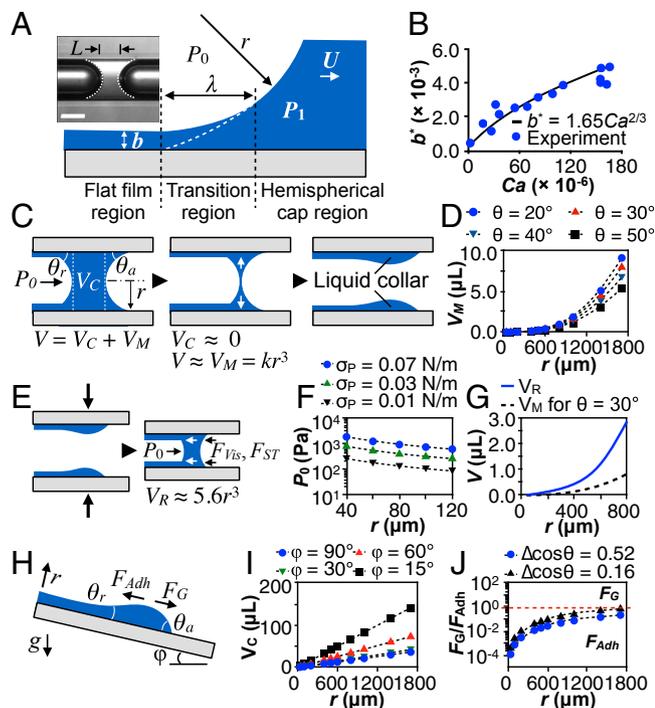
Liquid Plug Transport and Film Deposition in a Tube. When a liquid plug travels at a velocity U under a pressure P_0 in a tube with inner radius r, a liquid film with thickness b is generated on the tube surface at a distance λ from the receding plug meniscus (Fig. 2A). For a liquid plug in the surface tension-dominated regime (i.e., $Ca = \mu U/\sigma_P << 1$, where Ca, μ, and σ_P denote plug capillary number, viscosity, and surface tension, respectively), b can be determined from the forces acting on the plug. The balance of the viscous force $F_{Vis} \sim \mu U/b^2$ and the surface tension force $F_{ST} \sim \Delta P/\lambda$, where $\Delta P = P_0 – P_1 = \sigma_P/r$ is the Laplace pressure at the plug meniscus, leads to $b^2/r \sim \lambda Ca$. By matching the curvatures of the static meniscus $1/r$ in the hemispherical cap region and the dynamic meniscus b/λ^2 in the transition region, the length of the transition region becomes $\lambda = (br)^{1/2}$. Thus, the dimensionless film thickness, a ratio of the film thickness to the tube radius (27, 28), is $b^* = b/r \sim Ca^{2/3}$. By instilling plugs of deionized (DI) water into a glass tube, we experimentally verified the relationship $b^* = 1.6Ca^{2/3}$ (Fig. 2B and *SI Appendix*, Fig. S1 and Movie S1).

Plug rupture volume in a tube. A liquid plug traveling along a tube decreases its volume due to deposition of a liquid layer and eventually ruptures, producing a liquid collar (21, 29) (Fig. 2C). The total volume V of a plug is a sum of the volumes of the cylindrical part V_C and the menisci at both ends of the plug V_M: $V = V_C + V_M$. A liquid plug ruptures when $V \sim V_M$, that is, when $V_C \sim 0$ due to film deposition. $V_C = \pi r^2 L$, where L is the plug length measured from the menisci and $V_M = kr^3$, where $k = \pi(1 – \sin\theta)/\cos\theta – \pi/3[(1 – \sin\theta)/\cos\theta]^3$, with θ being the contact angle of the advancing and receding menisci (30). To determine the effect of the contact angle on the plug meniscus volume, k and V_M were calculated for various contact angles (e.g., $20° < \theta < 50°$) and tube radii (100 μm $< r <$ 1,000 μm) to show that k is inversely proportional to the contact angle and that an increase in θ will decrease V_M (*SI Appendix*, Fig. S2A). Because $V_M \sim r^3$, a greater meniscus volume is expected in a tube with a larger inner radius. V_M was measured for $20° < \theta < 50°$ and a range of lung airway diameters. Thus, in the $G_0–G_5$ region, a liquid plug ruptures when its volume falls below ~ 1 μL; in $\sim G_{15}$ region, a plug rupture volume can be as small as ~ 200 nL (Fig. 2D).

Plug travel distance in a tube. As a liquid plug with an initial volume V_0 travels a distance S in a tube, its volume becomes $V = V_0 – V_D = V_0 – SA_D$, where $A_D = \pi r^2 – \pi(r – b)^2$ is the cross-sectional area of the film. Because a plug ruptures when $V \sim V_M$, the plug can travel a total distance $S_{Total} \sim (V_0 – V_M)/A_D$. The experimental results we obtained using a glass capillary agree well with the theoretically determined S_{Total} which increases linearly with V_0, as larger plugs travel longer distances at the same Ca. Similarly, liquid plugs with greater Ca travel shorter distances, as they deposit thicker liquid film and lose their volumes faster (*SI Appendix*, Fig. S2 *B* and *C*).
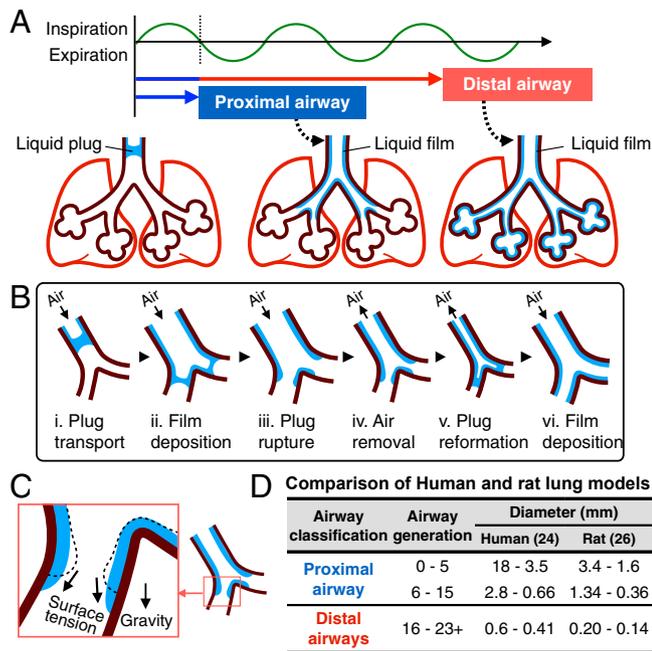
Fig. 1. Liquid film deposition in targeted generations of the pulmonary airway. (A) Liquid film deposition in a targeted region of the lung can be achieved by varying the initial plug volume and ventilation parameters. Liquid film can be delivered to the proximal airways by instilling a small liquid plug and inspiring air or to the distal airways by repeated cycles of plug transport, rupture, and reformation during continued ventilation. (B) Steps of the process: (i) Instillation of a liquid plug into an airway by positive air pressure. (ii) Liquid film deposition on the airway surfaces by moving plugs. (iii) Plug rupture on the airway surface. (iv) Decrease in airway diameters during expiration. (v) Plug reformation due to sufficient reduction in airway diameter. (vi) Continued film deposition by transport of reformed plugs. (C) Liquid film movement by surface tension gradient or gravity. (D) The proximal and distal airways of human and rat lung airways.

Comparison of Human and rat lung models

Airway classification	Airway generation	Diameter (mm)	
		Human (24)	Rat (26)
Proximal airway	0 - 5	18 - 3.5	3.4 - 1.6
	6 - 15	2.8 - 0.66	1.34 - 0.36
Distal airways	16 - 23+	0.6 - 0.41	0.20 - 0.14

Fig. 2. Liquid plug transport and film generation in a tube. (A) A liquid plug traveling in a tube with inner radius r deposits a liquid film with dimensionless thickness $b^* = b/r \sim Ca^{2/3}$. (Inset) Microscopic image of a liquid plug of a length L in a glass capillary. Dotted lines outline menisci. (Scale bar: 500 μm.) (B) A plug of DI water produced $b^* = 1.65Ca^{2/3}$ in a glass capillary. (C) A liquid plug ruptures and deposits a collar on the wall when its volume V reduces to the meniscus volume $V_M = kr^3$. V_M was obtained for various contact angles $20° < \theta < 50°$ and tube radii 100 μm $< r < 1,000$ μm representing rat airway diameters. (E) When r decreases, a plug can be reformed and moved distally under pressure P_0 against the resisting viscous force F_{Vis} and surface tension force F_{ST}. (F) P_0 was determined for various surface tension of liquid plug σ_P. (G) The plug reformation volume $V_R \sim 5.6r^3$ was calculated for smaller airways. (H) Liquid film can move on the airway surfaces by gravity force F_G against resisting adhesion force F_{Adh}. (I) Liquid collar volume V_C required for the gravity-driven film flow was calculated. (J) Ratio of F_G to F_{Adh} was determined to estimate their relative contributions to film flow.

Plug reformation and subsequent transport in a tube.

A liquid film deposited on the inner tube surface reforms into a new liquid plug when its volume exceeds a critical value (31). Due to the decreasing diameters in recoiling small airways, a liquid layer can thicken, become unstable, and reform into a new plug (Fig. 2E). To move the reformed plugs, P_0 must overcome the resisting surface tension force F_{ST} due to the contact angle hysteresis such that $P_0 > 2\sigma_P\Delta\cos\theta/r$, where $\Delta\cos\theta = \cos\theta_r - \cos\theta_a$. Because F_{ST} increases with decreased r and increased σ_P, greater P_0 is required to move plugs through smaller airways [e.g., a water plug moving in G_{16}–G_{23+}, with $\theta_r \sim 20°$ and $\theta_a \sim 65°$ (32)] (Fig. 2F). A liquid plug can reform in a tube when $V_R \sim 5.6r^3$ (31, 33). V_R calculated for tube radii corresponding to the smaller airways (e.g., G_6–G_{23+}) of the rat lung increases rapidly with r, showing that greater collar volume is required for plug reformation in airways with greater diameters. In a tube of radius r, $V_R > V_M$ ($V_M \sim 1.6r^3$ at $\theta = 30°$), liquid plug will reform following rupture when the radius r_1 of the airway decreases to $r_2 = 0.66r_1$ (Fig. 2G).

Liquid film movement by gravity.

Movement of liquid deposited on airway surfaces could be induced by gravity in the absence of the Marangoni effect (Fig. 2H). Gravity acting on the film is $F_G \sim \rho g V_C \sin\varphi$, where ρ is the liquid density, g is the gravity, V_C is the liquid collar volume, and φ is the inclined airway angle. The film adhesion force onto the surface is $F_{Adh} \sim \sigma\pi D\Delta\cos\theta$ (34). At various φ, V_C was calculated with $\Delta\cos\theta = 0.52$ (Fig. 2I), to show that a greater V_C is needed for the gravity to be significant in an airway with smaller incline angle φ and larger r. The ratio of gravity to the adhesion force calculated with $\varphi = 90°$ and $\Delta\cos\theta = 0.52$ and 0.16 showed that $F_G/F_{Adh} < 1$, indicating film formed in the airways would not move further distally as they can be held by the adhesion force on the surface (Fig. 2J).

Mathematical Model for Aqueous Liquid Film Delivery in the Rat Airways.

The architectural model for the rat airway was developed based on Weibel's human airway morphometry, with ~23 generations of dichotomous and symmetric branches from trachea (G_0) to alveoli (G_{23+}), and the number of airways $G_N = 2^N$ (23). Because plug rupture and reformation are determined by the decreasing airway diameters in the bronchial tree, we computed the diameters in a dimensionless form $d_N^* = d_N/d_0 = 2^{-N/Z}$, where d_N and d_0 are the diameters of G_N and G_0, respectively, and Z is a constant. Using rat airway diameters measured at total lung capacity (TLC ~ 12 mL) (26), we determined $Z = 4.3$ (Fig. 3A). In our approach, a liquid plug is instilled into the trachea of a rat lung maintained at residual volume (RV ~ 2 mL) and advanced into the airway by filling the lung with air to functional residual capacity (FRC ~ 6 mL) (35). We calculated $Z = 3.3$ and 3.75 for rat lungs at RV and FRC, respectively (Fig. 3B). The dimensionless cross-sectional area of G_N is $A_{Ntotal}^* = A_{Ntotal}/A_0 = 2^N d_N^{*2}$, where A_0 is the cross-sectional area of the trachea. Although d_N^* decreases when N increases, A_{Ntotal}^* increases because the number of airways increases as 2^N (*SI Appendix*, Fig. S3A). The dimensionless plug velocity is $U_N^* = U_N/U_0 = A_N^*/2^N$, where U_N and U_0 are the velocity of a plug in G_N and G_0, respectively, and decreases rapidly with G_N. Thus, a liquid plug will quickly slow down as it travels into more distal airways (*SI Appendix*, Fig. S3B).

Plug rupture and reformation in rat airways.

For a liquid plug of an initial volume V_0 and $Ca_0 = \mu U_0/\sigma$, the dimensionless thickness of the deposited film is $b_N^* = b_N/r_N = kCa_N^{2/3}$, where b_N is the film thickness; $Ca_N = Ca_0(r_0/r_N)^2/2^N$; and r_0 and r_N are the radii of G_0 and G_N airways, respectively. The dimensionless volume of the
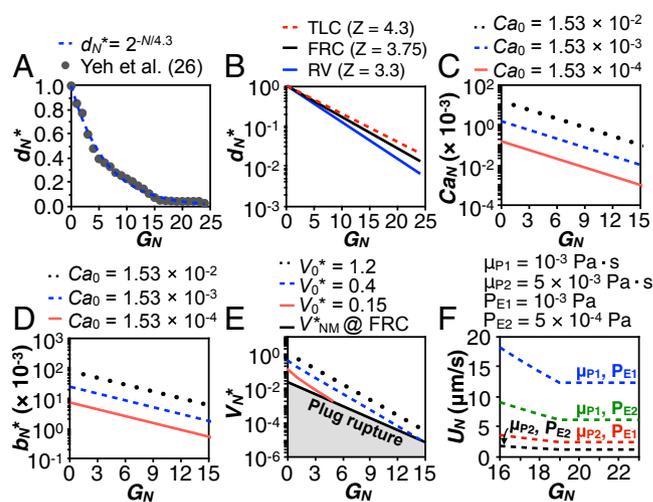
Fig. 3. Analysis of liquid plug transport and film generation in rat lungs. (A) At total lung capacity (TLC ~ 12 mL), airway diameters are a function of airway generation G_N as $d_N^* = d_N/d_0 = 2^{-N/4.3}$. (B) Similarly, airway diameters at residual air volume (RV ~ 2 mL) and functional residual capacity (FRC ~ 6 mL) are $d_N^* = 2^{-N/3.3}$ and $d_N^* = 2^{-N/3.75}$, respectively. (C–E) In the proximal airways (G_0–G_{15}), the capillary number is $Ca_0 = Ca_0(r_0/r_N)^2/2^N$ (C); the dimensionless film thickness is $b_N^* = kCa_N^{2/3}$, where $k = 1.6$ (D); and the dimensionless plug volume is $V_N^* = (V_0^* - \int_0^{N-1} V_{ND}dN)/2^N$, as shown for $V_0^* = 0.15, 0.4,$ and 1.2, and $Ca_0 = 1.53 \times 10^{-3}$ (E). (F) In the distal airways (G_{16}–G_{23+}), the plug speed U_N depends on the plug viscosity μ_P and effective pressure P_E.

liquid plug normalized to the trachea volume V_{Trachea} is $V_N^* = (V_0^* - \int_0^{N-1} V_{ND}^* dN)/2^N$, where $V_0^* = V_0/V_{\text{Trachea}}$ and $V_{ND}^* = V_{ND}/V_{\text{Trachea}}$, and V_{ND} is the liquid film volume in the G_N airway. As the liquid plug ruptures and forms a collar, its volume reduces to the meniscus volume $V_N^* \approx V_{NM}^* = k r_{N\text{FRC}}^3/V_{\text{Trachea}}$ at FRC, where $V_{NM}^* = V_{NM}/V_{\text{Trachea}}$ is the dimensionless meniscus volume and $r_{N\text{FRC}}$ is the radius of the G_N airway at FRC. As the lung volume reduces to RV during expiration, a liquid collar reforms into a plug when $V_{NR}^* = V_{NR}/V_{\text{Trachea}} \approx 5.6 r_{N\text{RV}}^3/V_{\text{Trachea}}$, where $r_{N\text{RV}}$ is the radius of G_N at RV. We simplified our analysis by assuming that liquid plugs travel and rupture under positive pressure when lung volume is approximately FRC, and plugs reform when lung volume nears RV. The meniscus contact angle was estimated as $\theta \sim 30°$ based on experimental data we collected, yielding $k = 1.6$.

Application of the model to the proximal rat airways (G_0–G_{15}). The effects of airflow rate on film deposition were measured at $Ca_0 = 1.53 \times 10^{-4}$, 1.53×10^{-3}, and 1.53×10^{-2}, by infusing 4 mL of air over 40 s, 4 s, or 0.4 s (from RV to FRC), respectively. A higher airflow rate at G_0 produces greater Ca_N in more distal airways (Fig. 3C). Ca_N decreases rapidly with N as plugs quickly slow down as they enter smaller airways, due to $A_{N\text{total}}^*$ increasing exponentially with N (*SI Appendix*, Fig. S3 *A* and *C*). b_N^* is greater in larger airways, and a thicker film is generated on the airway surface for greater Ca_0 (Fig. 3D). The volume of liquid deposited $V_{D\text{total}}^* = \int_0^N V_{ND}^* dN$ in the conducting airways of the rat also increases with Ca_0 (*SI Appendix*, Fig. S3C).

To achieve uniform film thickness in the conducting airways, the liquid plug should be advanced in the surface tension-dominant flow regime so that it experiences minimal effects of inertia and gravity. At a bifurcation, a fast-moving plug will tend to preferentially enter an airway oriented in the direction of the plug's pathway, due to inertia. Larger plugs (≥ 200 μL in the rat main bronchus) will enter airway branching in the direction of gravity, thus compromising uniformity of delivery. The relative significance of gravity and inertia to surface tension can be determined using the Bond number ($Bo = \rho g d^2/\sigma$) and the Weber number ($We = \rho U^2 d/\sigma$), respectively (21). Because $Bo > 1$ in larger airways (G_0 and G_1), the displacement vector of a liquid plug will be biased in the direction of gravity (*SI Appendix*, Fig. S4A). Similarly, $We > 1$ for high airflow rates (e.g., $We_0 = 57 >> 1$ for $Ca_0 = 1.53 \times 10^{-2}$) (*SI Appendix*, Fig. S4B). At lower airflow rates, surface tension dominates plug transport throughout airways, including larger airways ($We_0 = 5.7 \times 10^{-3} << 1$ for $Ca_0 = 1.53 \times 10^{-4}$). Thus, a liquid plug should be instilled at small Ca_0 to avoid inertial effects.

To demonstrate that liquid film can be deposited in target regions of the proximal airways, we measured plug transport at various initial plug volumes (e.g., $V_0^* = 0.15$, 0.4, and 1.2) infused at $Ca_0 = 1.53 \times 10^{-3}$. The model predictions were based on the assumption that a liquid plug ruptures when $V_N^* \sim V_{NM}^*$ (Fig. 3E). We show that deposition of liquid film can be achieved by selecting the initial plug volume. A plug with $V_0^* = 0.15$ and 0.4 traveled and ruptured after reaching G_5 and G_{15}, representing film deposition in G_0–G_5 and G_0–G_{15}, respectively. In contrast, a plug with $V_0^* = 1.2$ could reach G_{15} without rupturing, which is not desirable because it would not allow distal movement of plugs that requires plug rupture and reformation processes.

Application of the model to the rat distal airways (G_{16}–G_{23+}). In smaller airways, surface tension differences between liquid plugs and the pulmonary liquid (e.g., mucus and surfactant) lining on the airways could be energetically unfavorable for the distal movement of plugs. However, the pulmonary liquid interacts with instilled liquid plugs by convective and diffusive mixing (36), which results in continuously lowered surface tension of the plugs during their journey down the airways. Consequently, the difference in surface tension between the plug and the airway lining decreases,

and film deposition on the surface can be achieved at a lower flow resistance. On the other hand, the viscosity of aqueous liquid would increase due to the interaction with the pulmonary lining (37) and slow down plug motion in the airway at a given pressure. Assuming the plug movement follows Poiseuille's law in a tube, the speed of a plug in an airway is $U_N = (r_N^2/8\mu_P L_P)P_E$, where a positive pressure $P_E = P_0 - 2\sigma_P(\cos\theta_r - \cos\theta_a)/r_N$ is required to move the plug (38) (Fig. 3F). Various combinations of μ_P and P_E were tested to determine the U_N of liquid plugs with $L_P \sim 50$ μm. In general, P_E required to move plugs at a certain speed would increase in smaller airways and at higher liquid viscosity.

Phase diagrams for film deposition in the rat lung. For the proximal airways, we developed a $Ca_0 - V_0^*$ phase diagram defining the airway generation to which a plug introduced in the trachea will travel at given instillation conditions (*SI Appendix*, Fig. S5A). Our model shows that liquid film deposition into selected airways can be achieved using predefined plug volumes and instillation conditions. The minimum liquid volume needed to form a plug in the rat trachea was calculated using $V_{NR}^* \approx 5.6 r^3/V_{\text{Trachea}}$. Because $V_{\text{Trachea}} \sim 250$ μL, at least $V_0^* \approx 0.1$ (i.e., 10% of the trachea volume) is required for plug formation. Increasing Ca_0 results in plugs traversing fewer airways due to the deposition of a thicker film at a higher airflow rate. In general, a plug can reach deeper airways for greater V_0^* and smaller Ca_0 during instillation. Although a small Ca_0 would result in nonbiased delivery of a liquid film, its magnitude may need to be carefully determined to optimize delivery and therapeutic effect.

For the rat distal airways, we developed a phase diagram that shows the total time $\sum t_N \sim 2^N L_N A_N/(U_0 A_0)$ required to deposit liquid film from G_0 to all of the way into G_{23+} as a function of the effective pressure P_E and plug viscosity μ_P (*SI Appendix*, Fig. S5B). The lungs were assumed to be ventilated continuously at $Ca_0 = 1.53 \times 10^{-3}$ to study drug delivery under physiologically relevant conditions. Because μ_P and P_E largely determine the time required for film deposition, these two values could be modulated to complete the film deposition process within a desired time.

Film Deposition in Target Regions of the Rat Lung. Deposition of liquid film in the rat airway was experimentally verified using indocyanine green (ICG) fluorescent dye (excitation/emission: 785 nm/830 nm) in DI water visualized by near-infrared (NIR) imaging (39, 40). Following instillation of a predefined liquid volume via a catheter in the rat trachea, the fluorescent signal was measured in situ through the ventral surface of the lung. Liquid film deposition on alveolar surfaces was confirmed using fluorescent microbeads (1-μm diameter, excitation/emission: 580 nm/605 nm) (Fig. 4A and Movie S2). The menisci of ICG plugs in the left main stem bronchus were visualized by NIR imaging, confirming the contact angle $\theta \sim 30°$ used in our plug transport model (*SI Appendix*, Fig. S6).

Liquid film deposition in selected regions of the rat proximal airways. We first demonstrated targeted delivery of liquid film into two different regions in the proximal airways based on flow parameters shown in *SI Appendix*, Fig. S5A. ICG liquid plugs [$\sigma \sim 62$ mN/m (22)] with initial volumes $V_0 \sim 35$ μL or 110 μL were instilled by infusing 4 mL of air for 4 s ($Ca_0 = 1.53 \times 10^{-3}$) for targeted film deposition within the large airways (target region: G_0–G_5) or into the small airways (target region: G_0–G_{15}), respectively (Fig. 4B). Control lungs that were not instilled with plugs displayed no fluorescence. In lungs instilled with 35-μL-volume plugs, the fluorescence signal showed that the length of the airways covered with film from the carina was ~1.3 cm, indicating that the plug traveled from G_0 to ~G_5 and deposited liquid film before it ruptured. Instillation of 110-μL-volume plugs resulted in spatially uniform deposition throughout the lung, indicating penetration of liquid into smaller airways (*SI Appendix*, Fig. S7). Following instillation, lungs were ventilated, showed no regions of atelectasis, and recoiled without an increase in airflow resistance, suggesting negligible change in lung compliance and
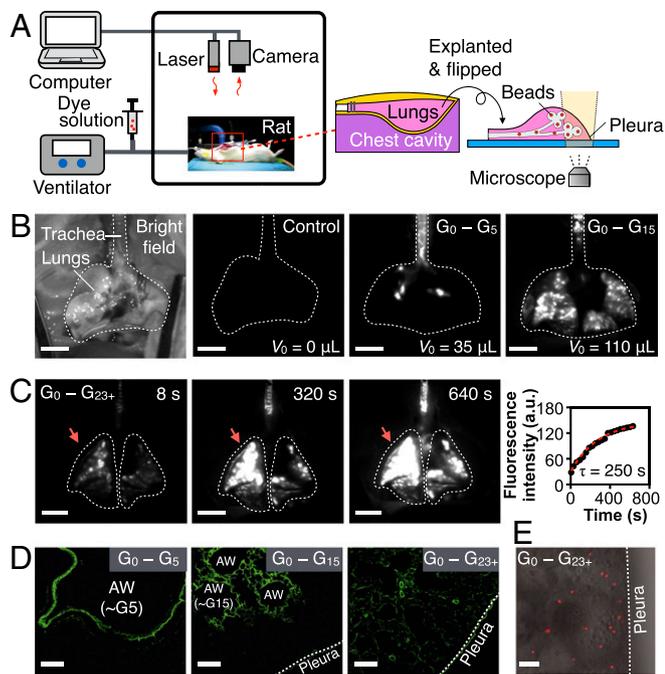
Fig. 4. Liquid film deposition in targeted regions of the rat airway. (*A*) Near-infrared (NIR) imaging was used to visualize liquid film deposition on airway surfaces by instilling microliter-volume liquid plugs containing indocyanine green (ICG) dye. Confocal imaging was used to verify film deposition in alveoli by fluorescent microbeads. (*B*) Film deposition in $G_0–G_5$ (35-µL plug) and $G_0–G_{15}$ (110-µL plug) was verified by fluorescence imaging through the ventral aspect of the lung. (Scale bar: 1 cm.) (*C*) Film deposition into alveoli (i.e., $G_0–G_{23+}$) was verified by fluorescent imaging following instillation of a 110-µL plug and continuous air ventilation for ~10 min. Time constant τ of the fluorescence increase for plugs entering alveoli was determined to be ~250 s. (Scale bar: 1 cm.) (*D*) Fluorescent images of lung cross-sections confirming CFSE film deposition in $G_0–G_5$, $G_0–G_{15}$, and $G_0–G_{23+}$. (Scale bar: 200 µm.) (*E*) Liquid deposition into subpleural alveoli (i.e., $G_0–G_{23+}$) was confirmed using fluorescent microbeads. (Scale bar: 50 µm.)

indicating that all plugs had ruptured and deposited liquid film in the airways (Movies S3 and S4).

Liquid film deposition from the rat trachea to the distal airways. We then demonstrated liquid film delivery from the rat trachea all of the way into the distal airways (target region: $G_0–G_{23+}$) by instilling 110-µL-volume liquid plugs followed by air ventilation at 1 mL/s (Fig. 4*C*). During the first cycle of air ventilation, fluorescence was visible throughout the lungs, confirming deposition of liquid film from the trachea into the deeper lung. When lungs were ventilated continuously, the fluorescence intensity increased as liquid advanced to the distal airways via repeated plug reformation and rupture until reaching the alveolar sacs (Movie S5). Because the ventral surface of the right upper lobe of the lung (Fig. 4*C*, arrow) was perpendicular to the camera during the experiment, fluorescence change in that lobe was more apparent than in other parts of the lungs. As ventilation continued for ~10 min, the fluorescence intensity reached a maximum as the surfaces of alveolar sacs were coated with liquid film containing ICG, which could occur with a possible combination of μ_P and P_E (*SI Appendix*, Fig. S5*B*), and the measured time constant of film deposition was $\tau \sim 250$ s (*SI Appendix*, Fig. S8).

Confirmation of liquid film deposition in target airways. To more accurately determine the airways deposited with liquid film, we used liquid plugs containing carboxyfluorescein diacetate succinimidyl ester (CFSE), which fluorescently labeled the airway epithelium in contact with the liquid film (Fig. 4*D* and *SI Appendix*, Fig. S9). Fluorescent images of lung cross-sections showed

that when 35 µL of CFSE solution was instilled, fluorescent signal indicating film deposited was observed only in the large airways ($G_0–G_5$). On the other hand, fluorescence was detected throughout the proximal airways ($G_0–G_{15}$) of the lungs instilled with 110 µL of CFSE. Although no signal was seen in the vast majority of alveoli, some peribronchiolar alveoli surrounding the target airways showed fluorescence due to diffusion of CFSE from the target airways. Furthermore, delivery of 110 µL of CFSE followed by 10 min ventilation resulted in film deposition in the entire airway surfaces ($G_0–G_{23+}$), as indicated by uniform fluorescence throughout the lungs. The presence of fluorescence beads in the subpleural region also verified film deposition into alveoli. (Fig. 4*E* and *SI Appendix*, Fig. S10 and Movie S6). These results demonstrate that liquid film can be delivered to targeted generations of the lung by microvolume liquid instillation.

Discussion

We show that aqueous liquid containing soluble drugs can be delivered into targeted branches of the lung airway and deposited onto the lung epithelium. The method is based on instilling a specific microvolume of liquid into the upper airways and moving the plug by programmed air ventilation into a desired area of the lung (Fig. 1). The distance a plug travels can be modulated by the plug volume, liquid viscosity, and ventilation. To precisely define the plug volume and ventilation conditions necessary to reach a specific target area in the lung, we formulated and validated a mathematical model of plug transport in a tubular geometry (Fig. 2) and then in a rat airway model (Fig. 3). Three important model predictions are that (*i*) the thickness of the film depends on the capillary number of the plug, $b* \sim Ca^{2/3}$; (*ii*) the liquid plug traveling through a ventilated airway ruptures when its volume decreases to $V_M \sim kr^3$; and (*iii*) a ruptured plug can reform into a new plug as airways recoil during exhalation such that $V_R \sim 5.6r^3$. Despite the complexities of the lung fluid mechanics, the volume and capillary number of the liquid plug at the point of instillation determined in capillary tube experiments can be applied to achieve targeted delivery into the proximal rat airways. In addition, the time required for film delivery into the distal rat airways was determined from the studies of the viscosity and surface tension of liquid plugs. To validate the mathematical model, we demonstrated deposition of liquid film in three different target regions (i.e., $G_0–G_5$, $G_0–G_{15}$, and $G_0–G_{23+}$) of the rat lung by three different imaging modalities (Fig. 4).

The collected data suggest the need to further refine our approach, which was developed using simplified rat airway geometries adapted from Weibel's model. The complex hierarchical structures and flow patterns in the rat airways affect the distribution of liquid film (23, 26) in a way not fully accounted for by our model. The effects of airway bifurcations on plug transport have not been considered, and it was assumed that liquid plugs split evenly at the airway branches. In reality, liquid plugs would split at bifurcations depending on their shape and surface properties (41). Also, plug rupture and reformation at airway bifurcations could be different from those in the tubular sections of the airway (21). Interaction between plugs and the airway walls during air ventilation would also need to be carefully studied to enable more accurate liquid delivery in actual lungs (21, 42). Although it would be technically challenging, the contact angles of liquid plugs and collars would need to be more precisely determined in the airways, especially within distal airways and alveoli. Because human lungs are considerably different from rat lungs in their surface properties [i.e., surface tension and mucus consistency (25, 26)], further studies are needed to extend the current study to the human lung. To improve drug delivery using this approach, diffusion of a given drug through the pulmonary liquid layer and into the epithelium (43) would also need to be characterized.

Clinical pulmonary drug delivery could be facilitated by refining procedures for plug instillation into the lung. Potentially, a multilumen balloon catheter could be inserted near a target region and used to deposit drug onto the isolated airway surfaces, while the patient is supported by gas exchange in other parts of the lung. In addition, novel techniques would be needed to precisely monitor film deposition in the human lungs, in particular for submicrometer thick films within complex airway structures that are below the threshold of conventional imaging (44). Drugs contained in the liquid film could more effectively diffuse and absorb into the epithelium, improving therapeutic effects. Optimal outcomes would result from the clearance of mucus before plug instillation (e.g., by the delivery of mucolytics or lung lavage) (36).

The clinical utility of this liquid delivery approach could extend to treating lung cancer and a range of acute and chronic pulmonary diseases. For example, high concentrations of mucoactive agents instilled with liquid plugs could help dissolve the mucus layer formed in the airways by many lung diseases, reducing complications and providing long-term benefits (45). For single cancer lesions, microvolume plugs containing high concentrations of chemotherapeutics can be delivered directly to the site of the tumor as a (neo)adjuvant therapy, especially for poorly vascularized tumors that are less accessible to systemically administered drugs. In addition, micrometastases in different and distal regions of the lung could also be treated by precise instillation of chemotherapeutics in conjunction with drugs given systemically. Bronchiectasis—permanent enlargement of an airway—caused by a number of acquired or infective diseases (e.g., tuberculosis, pneumonia, and cystic fibrosis) can result in secluded regions of airway that harbor pathogens that are extremely difficult to clear with orally or systemically administered antibiotics. In such cases, liquid plug instillation could be used to deliver high concentrations of antibiotics directly to infected sites. We envision that the theoretical and experimental studies presented here demonstrate that the instillation of liquid microvolumes could provide localized delivery of drugs at precisely known volumes and concentrations into targeted regions of the lung to treat a wide range of lung diseases.

Materials and Methods

Detailed methods can be found in *SI Appendix*. Briefly, liquid film deposition in a glass capillary was achieved by moving introduced DI water plugs via air pressure applied using a syringe pump. Depositions of liquid in the rat airways and alveoli were verified using fluorescent imaging of water film containing ICG and fluorescently labeled microbeads, respectively. Liquid film deposition in target airways was further demonstrated by delivering liquid plugs containing CFSE, which was confirmed using fluorescent microscopy. Rats were maintained in accordance with the Columbia University Institutional Animal Care and Use Committee standards and review.

1. Conway SP, Brownlee KG, Denton M, Peckham DG (2003) Antibiotic treatment of multidrug-resistant organisms in cystic fibrosis. *Am J Respir Med* 2(4):321–332.
2. Johnstone RW, Ruefli AA, Lowe SW (2002) Apoptosis: A link between cancer genetics and chemotherapy. *Cell* 108(2):153–164.
3. Albert RK, Spiro SG, Jett JR (2008) *Clinical Respiratory Medicine* (Elsevier, Philadelphia).
4. Mason RJ, et al. (2010) *Murray and Nadel's Textbook of Respiratory Medicine: 2-Volume Set* (Elsevier, Philadelphia).
5. Pond SM, Tozer TN (1984) First-pass elimination. Basic concepts and clinical consequences. *Clin Pharmacokinet* 9(1):1–25.
6. Chollet P, Favrot MC, Hurbin A, Coll JL (2002) Side-effects of a systemic injection of linear polyethylenimine-DNA complexes. *J Gene Med* 4(1):84–91.
7. Edwards DA, et al. (1997) Large porous particles for pulmonary drug delivery. *Science* 276(5320):1868–1871.
8. Labiris NR, Dolovich MB (2003) Pulmonary drug delivery. Part I: Physiological factors affecting therapeutic effectiveness of aerosolized medications. *Br J Clin Pharmacol* 56(6):588–599.
9. Hoppentocht M, Hagedoorn P, Frijlink HW, de Boer AH (2014) Technological and practical challenges of dry powder inhalers and formulations. *Adv Drug Deliv Rev* 75: 18–31.
10. Finlay WH (2001) *The Mechanics of Inhaled Pharmaceutical Aerosols: An Introduction* (Academic, London).
11. Cox CA, Cullen AB, Wolfson MR, Shaffer TH (2001) Intratracheal administration of perfluorochemical-gentamicin suspension: A comparison to intravenous administration in normal and injured lungs. *Pediatr Pulmonol* 32(2):142–151.
12. Patton JS, Fishburn CS, Weers JG (2004) The lungs as a portal of entry for systemic drug delivery. *Proc Am Thorac Soc* 1(4):338–344.
13. Tooley W, Clements J, Brown L (1987) Lung function in prematurely delivered rabbits treated with a synthetic surfactant1, 2. *Am Rev Respir Dis* 136(3):651–656.
14. Cochrane CG, Revak SD (1991) Pulmonary surfactant protein B (SP-B): Structure-function relationships. *Science* 254(5031):566–568.
15. Hawgood S, Clements JA (1990) Pulmonary surfactant and its apoproteins. *J Clin Invest* 86(1):1–6.
16. Zasadzinski J, Ding J, Warriner H, Bringezu F, Waring AJ (2001) The physics and physiology of lung surfactants. *Curr Opin Colloid Interface Sci* 6(5):506–513.
17. Luecke T, et al. (2006) Oleic acid vs saline solution lung lavage-induced acute lung injury: Effects on lung morphology, pressure-volume relationships, and response to positive end-expiratory pressure. *Chest* 130(2):392–401.
18. Espinosa FF, Shapiro AH, Fredberg JJ, Kamm RD (1993) Spreading of exogenous surfactant in an airway. *J Appl Physiol* 75(5):2028–2039.
19. Hsu SH, Strohl KP, Jamieson AM (1994) Role of viscoelasticity in tube model of airway reopening. I. Nonnewtonian sols. *J Appl Physiol* 76(6):2481–2489.
20. Reifenrath R, Zimmermann I (1973) Surface tension properties of lung alveolar surfactant obtained by alveolar micropuncture. *Respir Physiol* 19(3):369–393.
21. Halpern D, Jensen OE, Grotberg JB (1998) A theoretical study of surfactant and liquid delivery into the lung. *J Appl Physiol* 85(1):333–352.
22. Ikagawa H, et al. (2005) Chemical toxicity of indocyanine green damages retinal pigment epithelium. *Invest Ophthalmol Vis Sci* 46(7):2531–2539.
23. Weibel ER, Gomez DM (1962) Architecture of the human lung. Use of quantitative methods establishes fundamental relations between size and number of lung structures. *Science* 137(3530):577–585.
24. Weibel ER (1963) *Morphometry of the Human Lung* (Academic, New York).
25. Yeh H-C, Schum GM (1980) Models of human lung airways and their application to inhaled particle deposition. *Bull Math Biol* 42(3):461–480.
26. Yeh HC, Schum GM, Duggan MT (1979) Anatomic models of the tracheobronchial and pulmonary regions of the rat. *Anat Rec* 195(3):483–492.
27. Bretherton F (1961) The motion of long bubbles in tubes. *J Fluid Mech* 10(2):166–188.
28. Aussillous P, Quéré D (2000) Quick deposition of a fluid on the wall of a tube. *Phys Fluids* 12(10):2367–2371.
29. Espinosa FF, Kamm RD (1999) Bolus dispersal through the lungs in surfactant replacement therapy. *J Appl Physiol* 86(1):391–410.
30. Lautrup B (2005) *Physics of Continuous Matter* (Inst of Phys, Bristol, UK).
31. Gauglitz P, Radke C (1988) An extended evolution equation for liquid film breakup in cylindrical capillaries. *Chem Eng Sci* 43(7):1457–1465.
32. Kamath Y, Dansizer C, Weigmann HD (1984) Surface wettability of human hair. I. Effect of deposition of polymers and surfactants. *J Appl Polym Sci* 29(3):1011–1026.
33. Kamm RD, Schroter RC (1989) Is airway closure caused by a liquid film instability? *Respir Physiol* 75(2):141–156.
34. De Gennes P-G, Brochard-Wyart F, Quéré D (2004) *Capillarity and Wetting Phenomena: Drops, Bubbles, Pearls, Waves* (Springer, New York).
35. Tazaki G, et al. (2006) Functional residual capacity and airway resistance in rats of COPD model induced by systemic hyaluronidase. *Tokai J Exp Clin Med* 31(3):125–127.
36. Henderson AJ (1994) Bronchoalveolar lavage. *Arch Dis Child* 70(3):167–169.
37. Lai SK, Wang Y-Y, Wirtz D, Hanes J (2009) Micro- and macrorheology of mucus. *Adv Drug Deliv Rev* 61(2):86–100.
38. Rose W, Heins R (1962) Moving interfaces and contact angle rate-dependency. *J Colloid Sci* 17(1):39–48.
39. Weissleder R (2001) A clearer vision for in vivo imaging. *Nat Biotechnol* 19(4):316–317.
40. Hillman EM, Moore A (2007) All-optical anatomical co-registration for molecular imaging of small animals using dynamic contrast. *Nat Photonics* 1(9):526–530.
41. Ody CP, Baroud CN, de Langre E (2007) Transport of wetting liquid plugs in bifurcating microfluidic channels. *J Colloid Interface Sci* 308(1):231–238.
42. Zheng Y, et al. (2009) Liquid plug propagation in flexible microchannels: A small airway model. *Phys Fluids* 21(7):071903.
43. Khanvilkar K, Donovan MD, Flanagan DR (2001) Drug transfer through mucus. *Adv Drug Deliv Rev* 48(2-3):173–193.
44. Conway J (2012) Lung imaging—Two dimensional gamma scintigraphy, SPECT, CT and PET. *Adv Drug Deliv Rev* 64(4):357–368.
45. Hurt K, Bilton D (2014) Inhaled interventions in cystic fibrosis: Mucoactive and antibiotic therapies. *Respiration* 88(6):441–448.